The cohesive frictional crack model applied to the analysis of the dam-foundation joint

The cohesive frictional crack model applied to the analysis of the dam-foundation joint

F. Barpi [a,*], S. Valente [a]

[a] *Dipartimento di Ingegneria Strutturale e Geotecnica, Politecnico di Torino, Corso Duca degli Abruzzi 24, 10129 Torino (Italy)*

Abstract

The mechanical behaviour of dam-foundation joints plays a key role in concrete dam engineering since it is the weakest part of the structure and therefore the evolutionary crack process occurring along this joint determines the global load bearing capacity. The reference volume involved in the above mentioned process is so large that it cannot be tested in a laboratory: structural analysis has to be carried on by numerical modelling. The use of the asymptotic expansions proposed by Karihaloo & Xiao (2008) at the tip of a crack with normal cohesion and Coulomb friction can overcome the numerical difficulties that appear in large scale problems when the Newton-Raphson procedure is applied to a set of equilibrium equations based on ordinary shape functions (Standard Finite Element Method). In this way it is possible to analyze problems with friction and crack propagation under the constant load induced by hydro-mechanical coupling. For each position of the fictitious crack tip, the condition $K_1 = K_2 = 0$ allows us to obtain the external load level and the tangential stress at the tip. If the joint tangential strength is larger than the value obtained, the solution is acceptable, because the tensile strength is assumed negligible and the condition $K_1 = 0$ is sufficient to cause the crack growth. Otherwise, the load level obtained can be considered as an overestimation of the critical value and a special form of contact problem has to be solved along the fictitious process zone. For the boundary condition analyzed (ICOLD benchmark on gravity dam model), after an initial increasing phase, the water lag remains almost constant and the maximum value of load carrying capacity is achieved when the water lag reaches its constant value.

Key words: Cohesive crack, Concrete, Dam, Fluid driven fracture, Foundation, Frictional crack, Fracture, Hydro mechanical coupling, ICOLD, Joint, Water lag

1 Nomenclature

- $\prime$: derivative with respect to z
- $a_{1n}, a_{2n}, b_{1n}, b_{2n}$: real coefficients
- $A_n = a_{1n} + i\, a_{2n}, B_n = b_{1n} + i\, b_{2n}$: complex coefficients
- $\alpha_1, \alpha_2, \ldots$: best fitting constants
- c: joint cohesion
- E: Young modulus
- ν: Poisson's ratio
- δ: crack sliding displacement
- δ_c: critical value of δ
- f_t: ultimate tensile strength
- G_F^{II}: conventional Mode II fracture energy
- h_{iff}: imminent failure flood water level (Fig. 3)
- $h_{ovt} = h_{iff} - h_c$: over-topping water heigth
- h_c: dam crest height (Fig. 3)
- i: imaginary unit, iteration number
- K_1: mode I stress intensity factor
- K_2: mode II stress intensity factor
- λ_i: eigenvalues
- κ: Kolosov constant
- $\mu = E/(2\,(1+\nu))$: shear modulus
- $\mu_f = \frac{-\tau_{xy}}{\sigma_y}|_{\theta=\pi}$: stress ratio used in the asymptotic expansion
- $\phi(z)$: analytic function
- Φ: Coulomb friction angle in joint failure criterion (Fig. 4)
- $\chi(z)$: analytic function
- p: water pressure along the crack (Fig. 3)
- t_n: traction along the crack (Fig. 3)
- r: polar coordinate
- σ_x: stress along x direction
- σ_y: stress along y direction
- σ_c: critical value of σ_y (corresponding to $w = 0$)
- τ_{xy}: tangential stress
- θ: polar coordinate
- u: displacement along x direction
- v: displacement along y direction
- w: crack opening displacement
- w_c: critical value of w
- $w_{eff} = \sqrt{w^2 + \delta^2}$: effective joint opening
- $w_{eff,c}$: critical value of w_{eff}
- $z = r\, \mathrm{e}^{i\,\theta}$: complex variable

* Corresponding author.
Email addresses: fabrizio.barpi@polito.it, silvio.valente@polito.it (S. Valente).

2 Introduction

The mechanical behaviour of dam-foundation joints plays a key role in concrete dam engineering since it is the weakest part in the structure and therefore the evolutionary crack process occurring along the joint determines the global load bearing capacity. In the scientific literature two problems on load-bearing capacity are discussed:

- the problem of sliding along a pre-existing compressed discontinuity (see, among others, Barton et al. (1985), Plesha (1987), Gens et al. (1990), Stupkiewicz & Mróz (2001)),
- the problem of crack initiation and propagation along an undamaged interface (see Carol et al. (1997), Červenka et al. (1998), Barpi & Valente (2008), Cocchetti et al. (2002))

The latter problem is discussed below in the framework of the cohesive crack models, introduced by Barenblatt (1959) and Dugdale (1960) for elastoplastic materials, and by Hillerborg et al. (1976) for quasi-brittle materials. In this model, the fracture process zone (due to degradation mechanisms such as plastic micro-voiding or micro-cracking) in front of the actual crack tip is lumped into a discrete line (two-dimensional) or plane (three-dimensional) and is represented by a nonlinear traction-separation law across this line or plane. When the tangential components of the tractions are present the solution can lose uniqueness. Therefore numerical difficulties occur if the Newton-Raphson procedure is applied to a set of equilibrium equations based on ordinary shape functions (Standard Finite Element Method). In order to overcome these difficulties Strouboulis et al. (2001) proposed an approximation which employs knowledge about the character of the solution (Generalized Finite Element Method). In this direction we take advantage from the work of Karihaloo & Xiao (2008) on the asymptotic fields at the tip of a cohesive crack. In this model frictional forces operate when the crack faces are open. Therefore, these forces are different from those operating in a contact problem. In this context Karihaloo & Xiao (2008) obtained asymptotic expansions at a cohesive crack tip analogous to the Williams (1957) expansions at a traction-free crack tip for any traction-separation law that can be expressed in a special polynomial form.

3 Polynomial cohesive law for quasi-brittle materials

In order to obtain the separable asymptotic field at a cohesive crack tip (in terms of r and θ functions, see Fig. 1) in quasi-brittle materials, Karihaloo & Xiao (2007) reformulate the softening law into the following polynomial form:

$$\frac{\sigma_y}{f_t} = 1 + \sum_{i=1}^{5} \alpha_i \left(\frac{w}{w_c}\right)^{\frac{2i}{3}} - \left(1 + \sum_{i=1}^{5} \alpha_i\right)\left(\frac{w}{w_c}\right)^4 \tag{1}$$

where σ_y and f_t are the stress normal to the cohesive crack faces and the uniaxial tensile strength, respectively; w and w_c are the opening displacement of the cohesive crack faces and the critical displacement at the real crack tip; α_i are fitting parameters. Equation 1 can represent a wide variety of softening laws. For example, Karihaloo & Xiao (2007) showed that the experimental results of Cornelissen et al. (1986) for normal concrete can be fitted very well by Eq. 1 with: $\alpha_1 = -0.872$, $\alpha_2 = -16.729$, $\alpha_3 = 67.818$, $\alpha_4 = -110.462$, $\alpha_5 = 83.158$ (see Fig. 2). The above mentioned shape coefficients are used in the present work.

4 Asymptotic fields at the tip of a crack with normal cohesion and Coulomb friction

The mathematical formulation follows closely that used by Karihaloo & Xiao (2008), so only a brief description will be given here. Muskhelishvili (1953) showed that, for plane problems, stresses and displacements in the Cartesian coordinate system (see e.g. Fig. 1) can be expressed in terms of two analytic functions $\phi(z)$ and $\chi(z)$ of the complex variable $z = re^{i\theta}$

$$\sigma_x + \sigma_y = 2[\phi'(z) + \overline{\phi'(z)}] \tag{2}$$

$$\sigma_y - \sigma_x + 2i\tau_{xy} = 2[\overline{z}\phi''(z) + \chi''(z)] \tag{3}$$

$$2\mu(u + iv) = \kappa\phi(z) - z\overline{\phi'(z)} - \overline{\chi'(z)} \tag{4}$$

where a prime denotes differentiation with respect to z and an overbar complex conjugate. In Eq. 4, $\mu = E/[2(1+\nu)]$ is the shear modulus; the Kolosov constant is $\kappa = 3-4\nu$ for plane strain and $\kappa = (3-\nu)/(1+\nu)$ for plane stress; E and ν are Young's modulus and Poisson's ratio, respectively.

For a general mixed mode I+II problem, the two analytic functions $\phi(z)$ and $\chi(z)$ can be chosen as series of complex eigenvalue Goursat functions (Sih & Liebowitz (1968))

$$\phi(z) = \sum_{n=0} A_n z^{\lambda_n} = \sum_{n=0} A_n r^{\lambda_n} e^{i\lambda_n\theta} \tag{5}$$

$$\chi(z) = \sum_{n=0} B_n z^{\lambda_n+1} = \sum_{n=0} B_n r^{\lambda_n+1} e^{i(\lambda_n+1)\theta} \tag{6}$$

where the complex coefficients are $A_n = a_{1n} + ia_{2n}$ and $B_n = b_{1n} + ib_{2n}$. The eigenvalues λ_n and coefficients a_{1n}, a_{2n}, b_{1n} and b_{2n} are real.

Substituting complex functions 5 and 6 into 2, 3 and 4, the complete series expansions of the displacements and stresses near the tip of the crack can be written:

$$2\mu\, u = \sum_{n=0} r^{\lambda_n} \Big\{ \kappa[a_{1n}\cos\lambda_n\theta - a_{2n}\sin\lambda_n\theta] + \lambda_n[-a_{1n}\cos(\lambda_n-2)\theta + a_{2n}\sin(\lambda_n-2)\theta] + (\lambda_n+1)[-b_{1n}\cos\lambda_n\theta + b_{2n}\sin\lambda_n\theta] \Big\} \tag{7}$$

$$2\mu\, v = \sum_{n=0} r^{\lambda_n} \Big\{ \kappa[a_{1n}\sin\lambda_n\theta + a_{2n}\cos\lambda_n\theta] + \lambda_n[a_{1n}\sin(\lambda_n-2)\theta + a_{2n}\cos(\lambda_n-2)\theta] + (\lambda_n+1)[b_{1n}\sin\lambda_n\theta + b_{2n}\cos\lambda_n\theta] \Big\} \tag{8}$$

$$\sigma_x = \sum_{n=0} r^{\lambda_n-1} \Big\{ 2\lambda_n[a_{1n}\cos(\lambda_n-1)\theta - a_{2n}\sin(\lambda_n-1)\theta] - \lambda_n(\lambda_n-1)[a_{1n}\cos(\lambda_n-3)\theta - a_{2n}\sin(\lambda_n-3)\theta] - (\lambda_n+1)\lambda_n[b_{1n}\cos(\lambda_n-1)\theta - b_{2n}\sin(\lambda_n-1)\theta] \Big\} \tag{9}$$

$$\sigma_y = \sum_{n=0} r^{\lambda_n-1} \Big\{ 2\lambda_n[a_{1n}\cos(\lambda_n-1)\theta - a_{2n}\sin(\lambda_n-1)\theta] + \lambda_n(\lambda_n-1)[a_{1n}\cos(\lambda_n-3)\theta - a_{2n}\sin(\lambda_n-3)\theta] + (\lambda_n+1)\lambda_n[b_{1n}\cos(\lambda_n-1)\theta - b_{2n}\sin(\lambda_n-1)\theta] \Big\} \tag{10}$$

$$\tau_{xy} = \sum_{n=0} r^{\lambda_n-1} \Big\{ \lambda_n(\lambda_n-1)[a_{1n}\sin(\lambda_n-3)\theta + a_{2n}\cos(\lambda_n-3)\theta] + (\lambda_n+1)\lambda_n[b_{1n}\sin(\lambda_n-1)\theta + b_{2n}\cos(\lambda_n-1)\theta] \Big\} \tag{11}$$

$$w = v\Big|_{\theta=\pi} - v\Big|_{\theta=-\pi} = \sum_{n=0} \frac{r^{\lambda_n}}{\mu}[(\kappa + \lambda_n)a_{1n} + (\lambda_n + 1)b_{1n}] \sin \lambda_n \pi \tag{12}$$

$$\delta = u\Big|_{\theta=\pi} - u\Big|_{\theta=-\pi} = \sum_{n=0} \frac{r^{\lambda_n}}{\mu}[(\lambda_n - \kappa)a_{2n} + (\lambda_n + 1)b_{2n}] \sin \lambda_n \pi \tag{13}$$

The imposition of continuity conditions on normal stress component of Eq. 10 ($\sigma_y|_{\theta=\pi} = \sigma_y|_{\theta=-\pi}$) along the cohesive zone gives:

$$(a_{2n} + b_{2n}) \sin(\lambda_n - 1)\pi = 0 \tag{14}$$

The imposition of continuity conditions on tangential stress component of Eq. 11 ($\tau_{xy}|_{\theta=\pi} = \tau_{xy}|_{\theta=-\pi}$) along the cohesive zone gives:

$$[(\lambda_n - 1)a_{1n} + (\lambda_n + 1)b_{1n}] \sin(\lambda_n - 1)\pi = 0 \tag{15}$$

Equations 14 and 15 are satisfied for $\sin(\lambda_n - 1)\pi = 0$ or for $b_{2n} = -a_{2n}$. In other words the asymptotic solutions can be collected in two classes. The first class is characterized by integer eigenvalues:

$$\lambda_n = n + 1, \quad n = 0, 1, 2 \ldots, \quad w = 0, \quad \delta = 0 \tag{16}$$

the second class is characterized by the remaining cases (non integer eigenvalues):

$$b_{2n} = -a_{2n}, \quad b_{1n} = -\frac{\lambda_n - 1}{\lambda_n + 1} a_{1n}, \quad w \neq 0, \quad \delta \neq 0 \tag{17}$$

The imposition of the Coulombian friction condition ($\tau_{xy}|_{\theta=\pi} = -\mu_f \, \sigma_y|_{\theta=\pi}$) along the cohesive zone, for the first class of solutions, gives:

$$\lambda_n = n + 1, \quad n a_{2n} + (n + 2)b_{2n} = -\mu_f (n + 2)(a_{1n} + b_{1n}) \quad n = 0, 1, 2 \ldots \tag{18}$$

and, for the second class of solutions, gives:

$$(\mu_f a_{1n} - a_{2n}) \cos(\lambda_n - 1)\pi = 0 \tag{19}$$

Since both factors in Eq. 19 may vanish independently of each other, it appears that, for the crack with normal cohesion and Coulombian friction, the eigenvalues and asymptotic fields are not unique. Additional assumptions have to be made to ensure uniqueness. Assuming that $\mu_f a_{1n} - a_{2n} \neq 0$, Eq. 19 gives:

$$\cos(\lambda_n - 1)\pi = 0, \quad \lambda_n = \frac{2n+3}{2}, \quad n = 0, 1, 2 \ldots \tag{20}$$

This assumption does not lead to any loss of generality. Now, it is possible to complete the expressions of the asymptotic fields.

In the case of integer eigenvalues, substituting Eq. 18 in 10 gives:

$$\sigma_y|_{\theta=\pm\pi} = -\frac{\tau_{xy}|_{\theta=\pm\pi}}{\mu_f} = \sum_{n=0} (n+2)(n+1) r^n (a_{1n} + b_{1n}) \cos(n\pi) \tag{21}$$

In the case of non-integer eigenvalues, substituting Eqs. 17 and 20 in 12 and 13 gives:

$$w = \sum_{n=0} \frac{r^{\frac{2n+3}{2}}}{\mu} \left[\left(\kappa + \frac{2n+3}{2} \right) a_{1n} + \frac{2n+5}{2} b_{1n} \right] \sin \frac{2n+3}{2} \pi \tag{22}$$

$$\delta = \sum_{n=0} \frac{r^{\frac{2n+3}{2}}}{\mu} \left[\left(\frac{2n+3}{2} - \kappa \right) a_{2n} + \frac{2n+5}{2} b_{2n} \right] \sin \frac{2n+3}{2} \pi \tag{23}$$

In Eq. 20 $n = -1$ corresponds to the singular terms, which are excluded a priori ($K_1 = K_2 = 0$).

5 The iterative solution procedure

For each position of the fictitious crack tip (shortening FCT) the following iterative procedure is applied:

$$\begin{bmatrix} w \\ \delta \end{bmatrix}^{i+1} = f\left(\begin{bmatrix} \sigma_y \\ \tau_{xy} \end{bmatrix}^{i} \right), \qquad \begin{bmatrix} \sigma_y \\ \tau_{xy} \end{bmatrix}^{i+1} = g\left(\begin{bmatrix} w \\ \delta \end{bmatrix}^{i+1} \right) \quad i = 0, 1, 2 \ldots \tag{24}$$

Since the material outside the fracture process zone (shortening FPZ) is linear, it is possible to compute the external load multiplier (h_{ovt}) and the tangential

stress at the FCT ($\tau_{xy,FCT}$) by imposing that the stress field is not singular (stress intensity factors $K_1 = K_2 = 0$). All these linear constraints are included in the operator f.

Since w,δ,σ_y,τ_{xy} are compatible with the asymptotic solution, operator g includes the constraints described by Karihaloo & Xiao (2008) and not repeated here.

At the first iteration ($i = 0$) $w = \delta = 0$ is assumed along the FPZ. According to this approach h_{ovt} and $\tau_{xy,FCT}$ are not defined *a priori* but are obtained from the analysis related to a pre-defined position of the FCT. If $\tau_{xy,FCT}$ is less than or equal to the local critical value, the solution obtained can be accepted. On the contrary, if $\tau_{xy,FCT}$ exceeds the local critical value, the associated load level can be seen as an overestimation of the real critical value which remains unknown. Of course it is possible to reduce the load level but in that case K_1 becomes negative, a contact problem arises along the FPZ and the dilatancy condition has to be imposed. This special form of contact problem is beyond the scope of the present work.

In the well established literature on mechanical behaviour of concrete joints (see Červenka et al. (1998)), softening depends only on $w_{eff} = \sqrt{w^2 + \delta^2}$. In the asymptotic expansion used, softening depends only on w. Therefore, during the iterative procedure, w_c changes as follows:

$$w_c^{i+1} = \sqrt{w_{eff,c}^2 - (\delta^i)^2} \tag{25}$$

In this model, the sliding rate ($\dot{\delta}$) is independent from the opening rate ($\dot{w}$). With the terminology commonly used in plasticity, we can say that the failure criterion adopted is non-associative.

6 Numerical example

As an example of application, the benchmark problem proposed in 1999 by the International Commission On Large Dams ICOLD (1999) was analyzed (dam height 80 m, base 60 m, see Fig. 3).

For simplicity, the same value of Young's modulus ($E = 32.5$ GPa) and Poisson's ratio ($\nu = 0.125$) was assumed. Figure 4 shows the Mohr envelope of peak and residual strength for the joint (cohesion c=0.7MPa, $\Phi = 30^o$). The stress σ_x is positive (tension) along the lower edge of the crack. Figure 4 shows its contribution to the achievement of the critical condition. As the crack grows, the value of σ_x at the FCT (also called T-stress) reduces. For conservative

reasons, the tensile strength of the joint and the related fracture energy are assumed as negligible. In case of linear softening the ICOLD benchmark suggests the assumption of a critical value of the crack sliding displacement equal to $\delta_c = 1$ mm in the case of $w = 0$. Since the shape of the softening law assumed in the present paper is based on the results of Cornelissen et al. (1986), the previous value was increased to δ_c=2.56 mm. This choice is motivated by keeping constant the fracture energy G_F^{II} in the case $w = 0$. Since the crack is open, beyond this value no stress transfer occurs.

6.1 Water lag

The well established literature on water driven fracture (see Desroches et al. (1994)) assumes that the water penetrates into the crack but does not reach the FCT. The fraction of FPZ not reached by the water is called *water lag*. According to the experimental results of Reich et al. (1994), it is assumed that the water penetrates into the FPZ up to the conventional knee point of the softening law ($w > w_{eff,c} \times 2/9 = 2.56 \times 2/9 = 0.569$ mm). At the points where the water penetrates, the pressure is the same as in the reservoir at the same depth. The concrete and the rock are assumed to be impervious. The asymptotic expansion used is based on the assumption $\tau_{xy}|_{\theta=\pi} = -\mu_f \sigma_y|_{\theta=\pi}$ therefore it can be applied only in the region not reached by the water. Figure 5 shows the evolution of the water lag as a function of the FCT position. The free parameters of the expansion are calibrated in this region. In the remaining part of the FPZ ordinary shape functions are used. For example, when the distance of the FCT from upstream edge is 15 m Figs. 6, 7 and 8 show that the total solution perfectly fits the asymptotic curve in terms of crack opening and sliding displacement and in terms of tangential cohesive stress (the normal component is negligible as required by the benchmark).

6.2 Loading conditions

The dam is analyzed under self-weight, reservoir filling and imminent failure flood loading conditions. In the numerical analysis the role of external load multiplier was played by the water level above the dam crest also called overtopping water heigth (shortening $h_{ovt} = h_{iff} - h_c$, see Fig. 3). Under the conservative assumptions previously described related to the material properties, the crack starts before the water level reaches the dam crest ($h_{ovt} < 0$).

Figure 9 shows the evolution of (τ/c) at the FCT as a function of the FCT position. Based on the foregoing discussion, we can conclude that the associated load level h_{ovt} shown in Fig. 10 is just an overestimation of the real level. This model behaviour is due to the low value of cohesion suggested by

the benchmark. For higher values of cohesion the solution shown in Fig. 11 and 10 is completely acceptable. Figure 10 gives the maximum value of h_{ovt} which is also the maximum load carrying capacity of the dam. Figure 11 shows the evolution of the horizontal crest displacement as a function of the FCT position and Fig. 12 the deformed mesh along the joint.

7 Conclusions

- The reference volume involved in the fracture process of a dam joint is so large that it cannot be tested in a laboratory: a numerical model is needed.
- The use of the asymptotic expansions proposed by Karihaloo & Xiao (2008) at the tip of a crack with normal cohesion and Coulomb friction can overcome the numerical difficulties that appear in large scale problems when the Newton-Raphson procedure is applied to a set of equilibrium equations based on ordinary shape functions (Standard Finite Element Method). The assumption of a different law of sliding, for which the asymptotic expansion is not available in the literature, can induce a very slow rate of convergence.
- In this way it is possible to analyze problems with friction and crack propagation under the constant load induced by hydro-mechanical coupling.
- In the analysis of the dam-foundation joint penetrated by the water, for each position of the FCT, the two conditions $K_1 = K_2 = 0$ allow us to obtain the external load level and the tangential stress at the FCT. If the joint strength is larger than the value obtained, the solution is acceptable, because the tensile strength is assumed negligible (according to the benchmark) and the condition $K_1 = 0$ is sufficient to cause the crack growth. Otherwise the load level obtained can be considered as an overestimation of the critical value.
- For the boundary condition analyzed, after an initial increasing phase, the water lag remains almost constant.
- For the boundary condition analyzed, the maximum value of load carrying capacity is achieved when the water lag reaches its constant value.

8 Acknowledgments

The financial support provided by the Italian Ministry of Education, University and Scientific Research (MIUR) to the research project on *"Structural monitoring, diagnostic inverse analyses and safety assessments of existing concrete dams"* (grant number 20077ESJAP_003) is gratefully acknowledged.

References

Barenblatt, G. (1959). The formation of equilibrium cracks during brittle fracture: general ideas and hypotheses, *Journal of Applied Mathematics and Mechanics* pp. 622–636.

Barpi, F. & Valente, S. (2008). Modeling water penetration at dam-foundation joint, *Engineering Fracture Mechanics* **75/3-4**: 629–642. Elsevier Science Ltd. (Great Britain).

Barton, N., Bandis, S. & Bakhtar, K. (1985). Strength, deformation and conductivity coupling of rock joints, *International Journal of Rock Mechanics and Mining Sciences* **22:33**: 121–140.

Carol, I., Prat, P. & Lopez, C. (1997). A normal/shear cracking model: Application to discrete crack analysis, *Journal of Engineering Mechanics (ASCE)* **123(8)**: 765–773.

Cocchetti, G., Maier, G. & Shen, X. (2002). Piecewise linear models for interfaces and mixed mode cohesive cracks, *Journal of Engineering Mechanics (ASCE)* **3**: 279–298.

Cornelissen, H., Hordijk, D. & Reinhardt, H. (1986). Experimental determination of crack softening characteristics of normal and lightweight concrete, *Heron* **31**: 45–56.

Desroches, J., Detournay, E., Lenoach, B., Papanastasiou, P., Pearson, J., Thiercelin, M. & Cheng, A. (1994). The crack tip region in hydraulic fracture, *Proceedings of the Royal Society of London A* **447**: 39–48.

Dugdale, D. (1960). Yielding of steel sheets containing slits, *Journal of Mechanics and Physics of Solids* **8**: 100–114.

Gens, A., Carol, I. & Alonso, E. (1990). A constitutive model for rock joints, formulation and numerical implementation, *Computers and Geotechnics* **9**: 3–20.

Hillerborg, A., Modeer, M. & Petersson, P. (1976). Analysis of crack formation and crack growth in concrete by means of fracture mechanics and finite elements, *Cement and Concrete Research* **6**: 773–782.

ICOLD (1999). Theme A2: Imminent failure flood for a concrete gravity dam, *Fifth International Benchmark Workshop on Numerical Analysis of Dams*, Denver (CO).

Karihaloo, B. & Xiao, Q. (2007). Accurate simulation of frictionless and frictional cohesive crack growth in quasi-brittle materials using xfem, *in* A. Carpinteri, P. Gambarova, G. Ferro & G. Plizzari (eds), *Sixth International Conference on Fracture Mechanics of Concrete and Concrete Structures (FRAMCOS6)*, Taylor and Francis (London), pp. 99–110.

Karihaloo, B. & Xiao, Q. (2008). Asymptotic fields at the tip of a cohesive crack, *International Journal of Fracture* **150**: 55–74.

Muskhelishvili, N. (1953). *Some basic problems of the mathematical theory of elasticity*, Noordhoof (Leyden).

Plesha, M. (1987). Constitutive models for rock discontinuities with dilatancy and surface degradation, *International Journal for Numerical and Analytical Methods in Geomechanics* **11**: 345–362.

Reich, W., Brühwiler, E., Slowik, V. & Saouma, V. (1994). Experimental and computational aspects of a water/fracture interaction, Balkema, The Netherlands, pp. 123–131.

Sih, G. & Liebowitz, H. (1968). Mathematical theories of brittle fracture, *in* H. Liebowitz (ed.), *Fracture (vol. II)*, Academic Press (New York), pp. 67–190.

Strouboulis, T., Copps, K. & Babuska, I. (2001). The generalized finite element method, *Computer Methods in Applied Mechanics and Engineering* **190**: 4081–4193.

Stupkiewicz, S. & Mróz, Z. (2001). Constitutive models for rock discontinuities with dilatancy and surface degradation, *Journal of Theoretical and Applied Mechanics* **3 (39)**: 707–739.

Červenka, J., Kishen, J. & Saouma, V. (1998). Mixed mode fracture of cementious bimaterial interfaces; part ii: Numerical simulations, *Engineering Fracture Mechanics* **60(1)**: 95–107.

Williams, M. (1957). On the stress distribution at the base of a stationary crack, *Journal of Applied Mechanics* pp. 109–114.

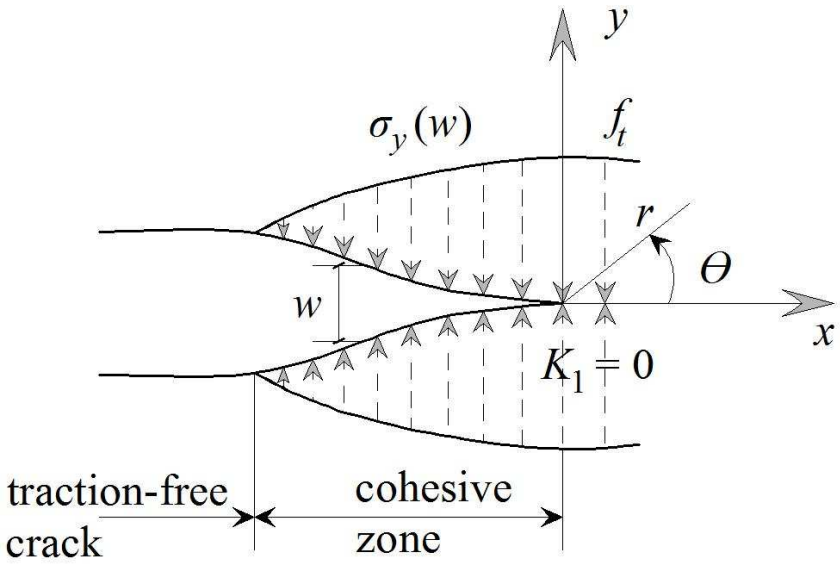

Fig. 1. Stresses near the crack tip.

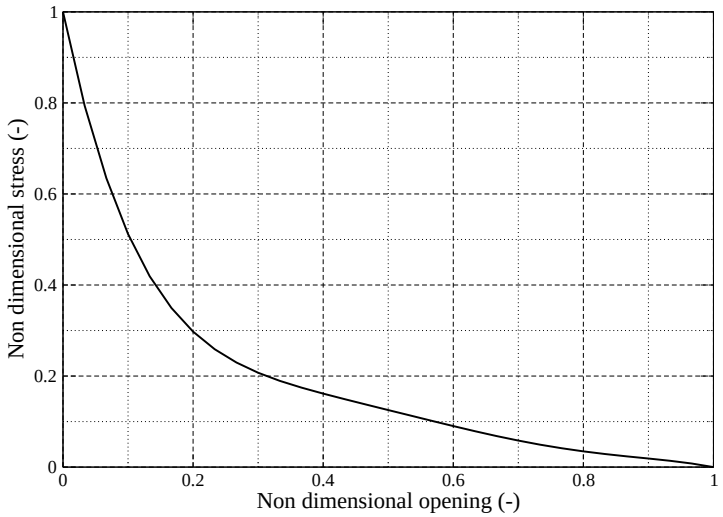

Fig. 2. Non dimensional cohesive stress (σ/σ_c) vs. non dimensional crack opening (w/w_c).

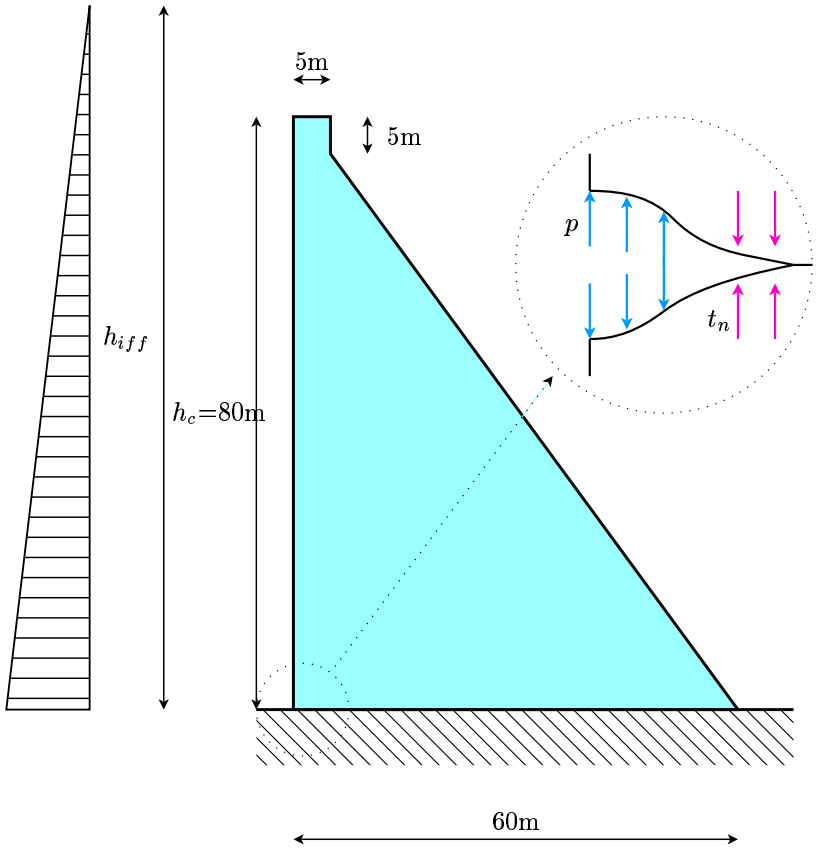

Fig. 3. Gravity dam proposed as benchmark by ICOLD (1999).

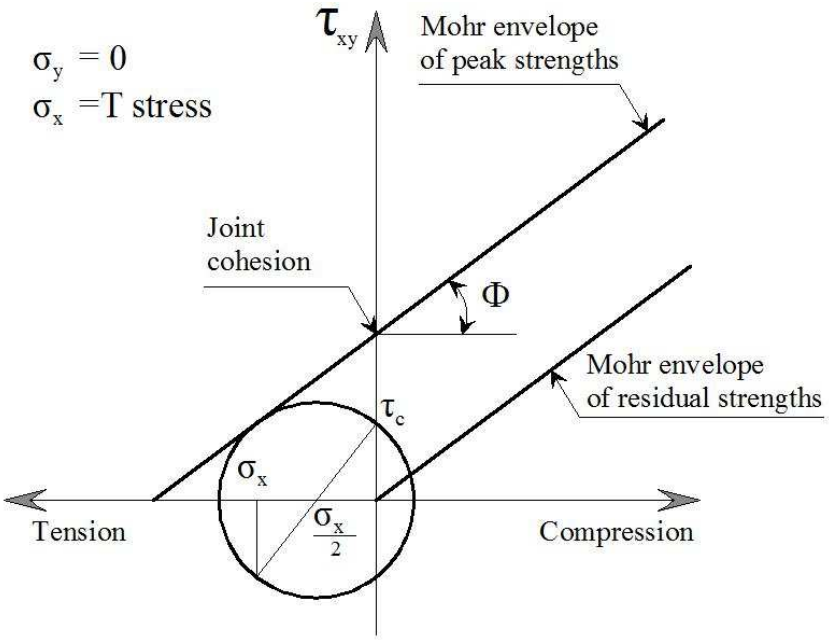

Fig. 4. Failure criterion.

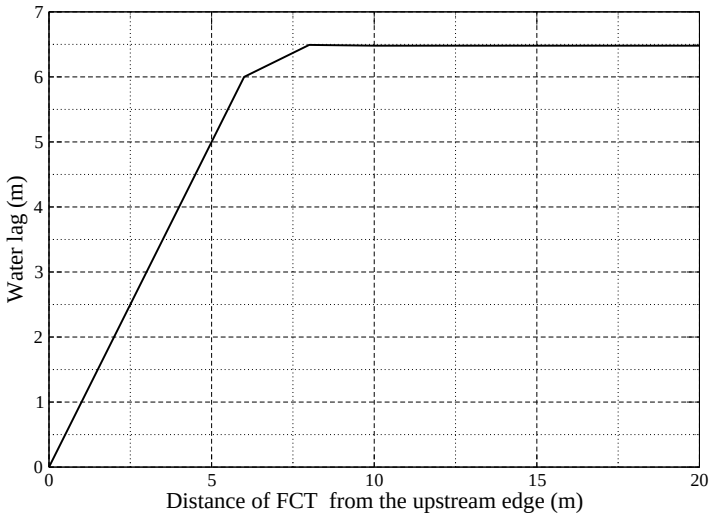

Fig. 5. Water lag vs. FCT position.

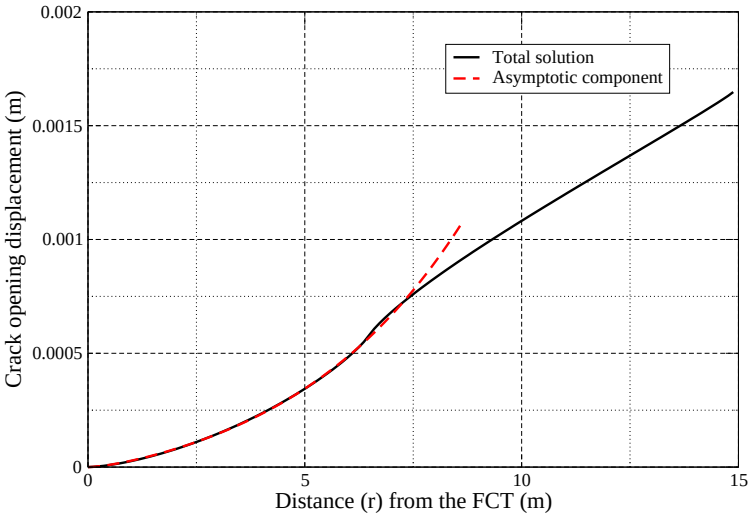

Fig. 6. Crack opening displacement vs. distance r.

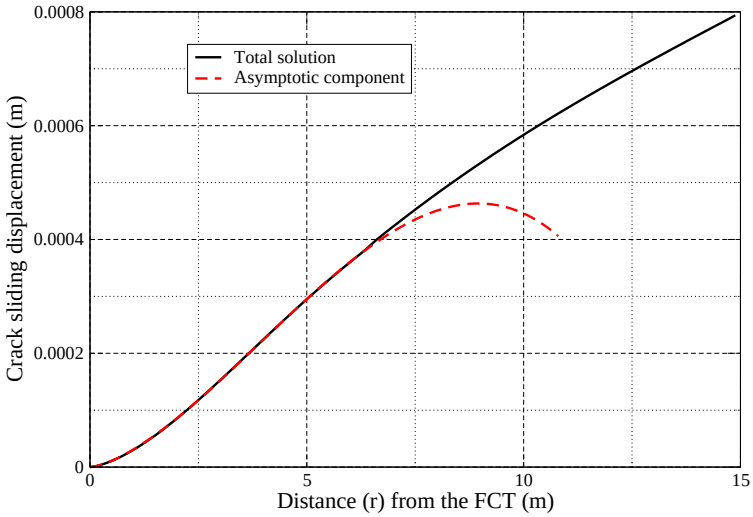

Fig. 7. Crack sliding displacement vs. distance r.

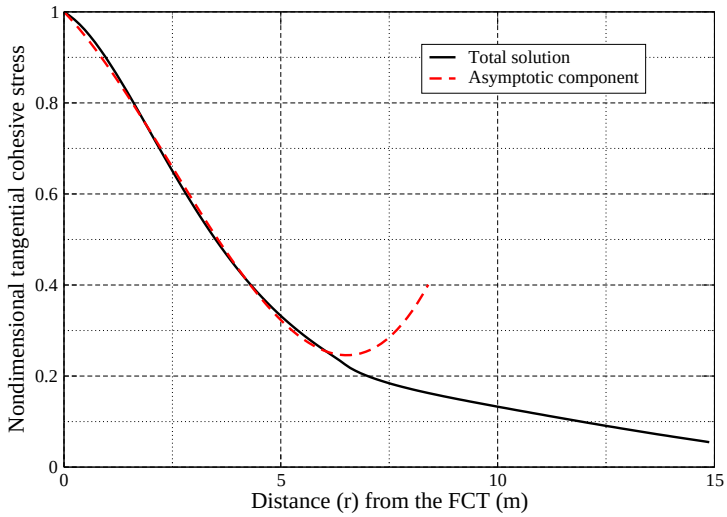

Fig. 8. Nondimensional tangential cohesive stress (τ/c) vs. distance r.

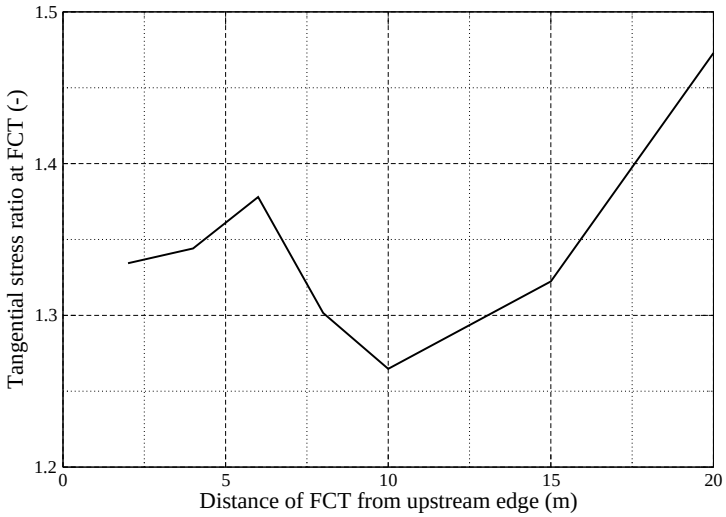

Fig. 9. Tangential stress ratio τ_{xy}/c at FCT vs. FCT position.

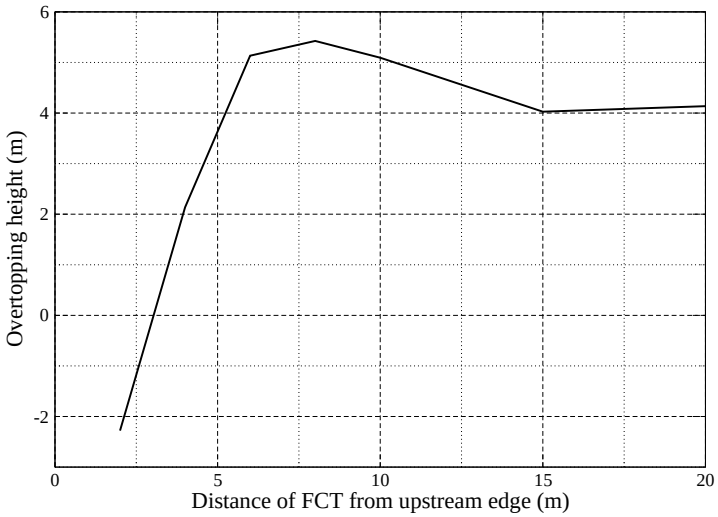

Fig. 10. Overtopping height h_{ovt} vs. FCT position.

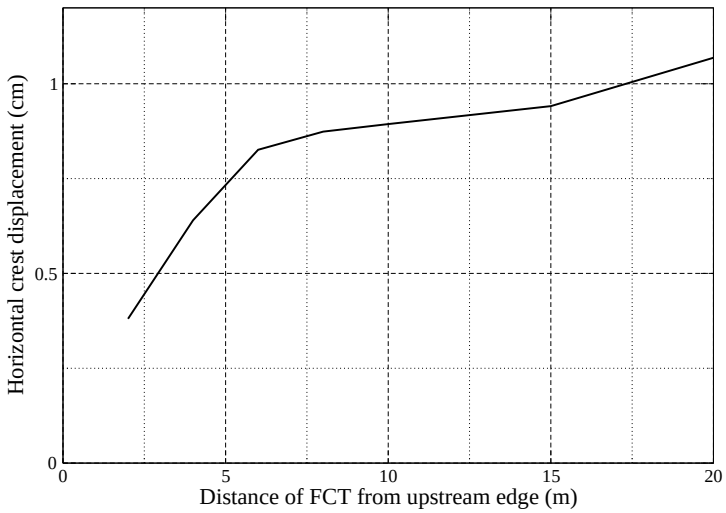

Fig. 11. Horizontal crest displacement vs. FCT position.

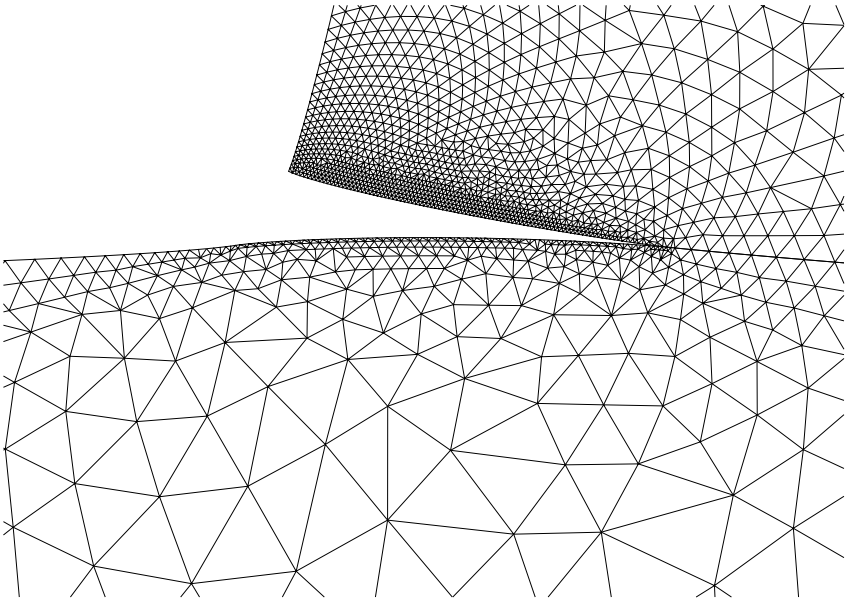

Fig. 12. Deformed mesh.